sustainability

Review

Recent Developments on Rare-Earth Hexaboride Nanowires

Zhen Wang [1] and Wei Han [2,*]

[1] School of Microelectronics, Southern University of Science and Technology, Shenzhen 518055, China; wangz8@sustech.edu.cn
[2] Department of Applied Physics, The Hong Kong Polytechnic University, Kowloon, Hong Kong 999077, China
* Correspondence: weihan@polyu.edu.hk

Abstract: With the rise of topological insulator samarium hexaboride (SmB_6), rare-earth hexaboride (RB_6) nanowires are the focus of the second wave of a research boom. Recent research has focused on new preparation methods, novel electronic properties, and extensive applications. Here, we review the recent developments in RB_6 nanowires in the past five years. Two main synthesis methods (chemical vapor deposition and high-pressure solid-state) of RB_6 nanowires are introduced and compared. Moreover, their electronic transport, magnetic properties, and superconducting properties are revealed. Furthermore, the applications of RB_6 nanowires are presented, including as field emitters, photodetectors, and in energy storage. Finally, we detail further research directions for RB_6 nanowires.

Keywords: rare-earth hexaboride; nanowire; field emission; chemical vapor deposition

check for updates

Citation: Wang, Z.; Han, W. Recent Developments on Rare-Earth Hexaboride Nanowires. *Sustainability* **2021**, *13*, 13970. https://doi.org/10.3390/su132413970

Academic Editor: Changhyun Roh

Received: 22 November 2021
Accepted: 14 December 2021
Published: 17 December 2021

1. Introduction

Rare-earth hexaborides (RB_6) have received substantial attention thanks to their high electrical conductivity, high melting points, and high chemical stability. Meanwhile, the strong correlation effect of 4f–5d electrons of rare-earth elements also brings some newfangled physical properties of RB_6 [1–3]. For example, yttrium hexaboride (YB_6) is a superconductor with a Tc of 7.2 K, which is the second highest transition temperature among all borides [4]. Moreover, lanthanum hexaboride (LaB_6), possessing low work function of 2.7 eV, is a famous thermionic electron emission material with high current density and stability [5]. Cerium hexaboride (CeB_6) is an antiferromagnetic heavy-fermion metal, but recently, it was found to demonstrate low-energy ferromagnetic fluctuation [6]. Furthermore, as a ferromagnetic semimetal, europium hexaboride (EuB_6) recently exhibited a colossal magnetoresistance effect [7]. In recent years, the emergent topological insulator has increased interest in samarium hexaboride (SmB_6), which possesses both insulating bulk state and metallic surface state due to the inversion of the d and f bands. Experimental evidence proves that SmB_6 is the first strongly correlated 3D topological Kondo insulator [8].

Due to the small size effect and quantum confinement effect, one-dimensional (1D) nanomaterials have new properties compared with bulk crystals. With the rise of 1D nanomaterials, RB_6 experienced the first wave of a research boom from 2005 to 2015, and many RB_6 nanowires were prepared by chemical vapor deposition (CVD) [9–20]. These RB_6 nanowires achieved excellent field emission properties and mechanical properties [21–29]. From 2016, the second wave of research boom of RB_6 began as SmB_6 proved to be a topological insulator, and researchers began to explore the difference in topological properties between nanowires and bulk single crystals [8].

In this review, we summarize the recent developments in RB_6 nanowires. Two main synthesis methods of RB_6 nanowires are summarized. Furthermore, their electronic transport and magnetic properties are summarized. Finally, the applications of RB_6 nanowires are presented, including as field emitters, photodetectors, and in energy storage.

2. Growth of RB_6 Nanowires

The structural models of rare-earth hexaborides are shown in Figure 1a. RB_6 crystals are CsCl-type structures with a space group of *Pm*-3*m*. Among 17 rare-earth elements, only 13 can form hexaborides with boron, which are YB_6, LaB_6, CeB_6, PrB_6, NdB_6, SmB_6, EuB_6, GdB_6, TbB_6, DyB_6, HoB_6, ErB_6, and YbB_6. On the left side of Figure 1a, one B_6 octahedron is surrounded by eight R atoms, and RB_6 crystals generally have suitable conductivity. On the right side of Figure 1a, one R atom is encircled by eight B_6 octahedra, and B_6 octahedra are connected by covalent bonds, which give RB_6 high melting points, high hardness, and high chemical stability. From the study of electronic structure and bonding characteristics of LaB_6, lanthanum and adjacent boron atoms are not sufficiently bonded, indicating that lanthanum atoms can migrate efficiently [30]. During the thermal field emission, the lanthanum atoms can freely migrate in the boron frame to replace the lanthanum atoms evaporated on the surface, thus showing excellent field emission performance [31]. Rare-earth hexaborides share common properties, but the special electronic structure of each material determines their characteristic properties. For instance, YbB_6 was once proposed to be a topological insulator, but new evidence for the electronic structure suggests that its electronic states originate from the hybridization of the Yb d- and B p-orbits. This indicates that YbB_6 has a non-topological insulator electronic structure [32]. Although most of the RB_6 crystals are metals, SmB_6 can open the band gap at low temperature due to the hybridization of the 4f bands and 5d bands, and meanwhile, metallic surface states are topologically protected [33]. To study and utilize the properties of RB_6, high-quality crystals, especially low-dimensional nanowires, need to be prepared. Concerning materials preparation, only two methods are reported to obtain RB_6 nanowires, chemical vapor deposition (CVD) and high-pressure solid-state (HPSS), as depicted in Figure 1b. CVD is a tradition method to grow RB_6 nanowires using vapor–liquid–solid (VLS) or vapor–solid (VS) mechanisms at a high temperature. HPSS using autoclave is a new method to grow RB_6 nanowires at a low temperature.

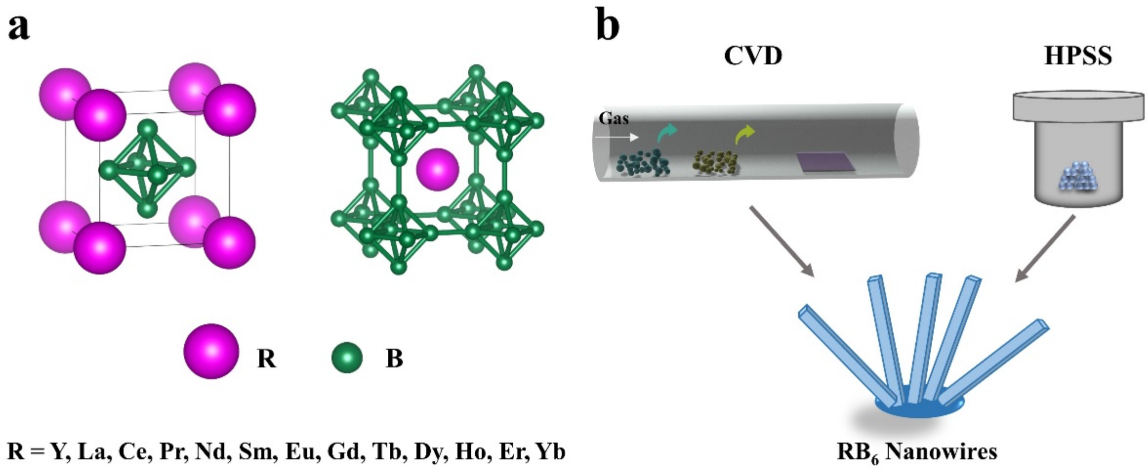

Figure 1. (**a**) The ball-and-stick structural models of rare-earth hexaborides. (**b**) Sketch map of two growth methods of RB_6 nanowires.

2.1. CVD Growth

In the past 5 years, a series of RB_6 nanowires were prepared by the CVD method, namely, LaB_6, CeB_6, NdB_6, SmB_6, and ternary $La_xPr_{1-x}B_6$ nanowires, as shown in Figure 2. Different methods use different source materials and substrates, as summarized below.

$$RCl_3 + B + B_2O_3 + H_2 \rightarrow RB_6 \text{ (R = La, Sm)} \quad (1)$$

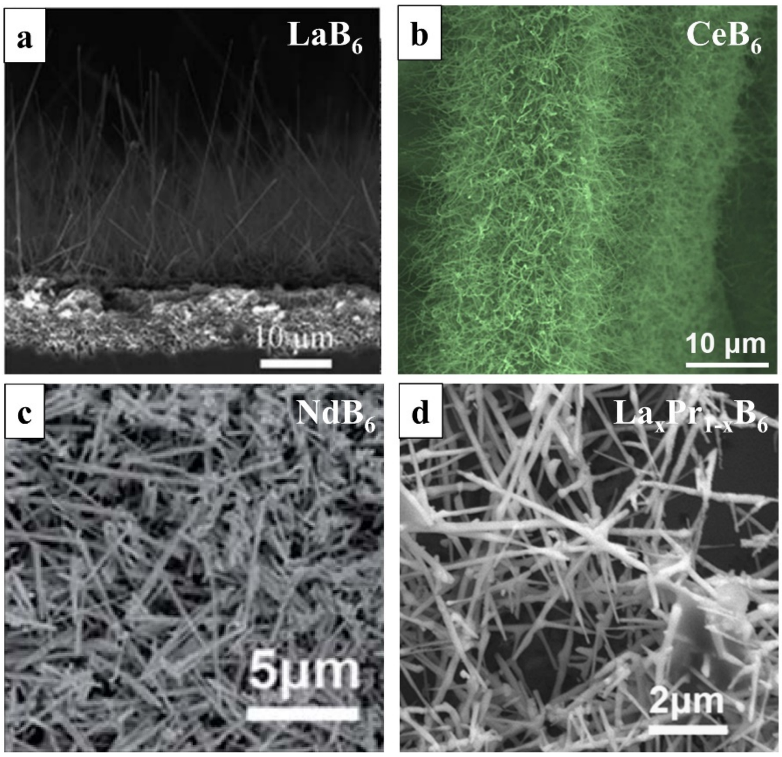

Figure 2. SEM images of (**a**) CVD-grown LaB_6 nanowires [34] (Copyright 2017, The Royal Society of Chemistry), (**b**) CeB_6 nanowires [35] (Copyright 2017, Elsevier Science B.V.), (**c**) NdB_6 nanowires [36] (Copyright 2016, The Royal Society of Chemistry), (**d**) $La_xPr_{1-x}B_6$ nanowires [37] (Copyright 2016, Elsevier Science B.V.).

From 2017 to 2019, Gan et al. used a Ni-catalyzed low-pressure CVD method to prepare high-quality LaB_6 and SmB_6 nanowires with a length of tens of microns, as depicted in Figure 2a [34,38]. The source materials of this method are $LaCl_3$ ($SmCl_3$), H_2, B, and B_2O_3, and they are non-toxic. Halides are common rare-earth sources, easy to decompose and reactive. The innovation of this method lies in the use of B and B_2O_3 as the boron source, because boron powder alone is extremely difficult to change to a gaseous state and has low reactivity. At a high temperature of 1000 °C, the mixture of B and B_2O_3 can produce active B_2O_2 vapor, and then B_2O_2 reacts with $LaCl_3$ ($SmCl_3$) and H_2 to grow LaB_6 and SmB_6 nanowires on Ni-coated Si substrates. The LaB_6 nanowires exhibit excellent field emission properties and stability, both at room temperature and at high temperatures [34]. Compared with bulk single crystals, the transport properties prove that SmB_6 nanowires have less residual resistance due to their large surface area [38].

$$CeCl_3 \cdot 7H_2O + B_2H_6 \rightarrow CeB_6 \quad (2)$$

In another method, Fu et al. applied a low-pressure CVD route to grow CeB_6 nanowires on Au-coated flexible carbon cloths using $CeCl_3 \cdot 7H_2O$ and B_2H_6 as source materials, as depicted in Figure 2b [35]. In this method, the $CeCl_3 \cdot 7H_2O$ is safe, but the B_2H_6 gas is deleterious to humans. The field emission properties of flexible CeB_6 nanowire arrays are outstanding, showing a low turn-on field and a high field emission enhancement factor. Meanwhile, the field current density can remain stable under bending conditions.

$$SmCl_3 + BCl_3 + H_2 \rightarrow SmB_6 \quad (3)$$

Besides B_2H_6 gas, BCl_3 gas is also a common source of gaseous boron. In 2016, Zhou et al. used a CVD route to grow SmB_6 nanowires on Au-coated Si substrates [39]. The electron transport testing on four-probe single-nanowire devices showed that the SmB_6

nanowire has a saturated resistance under 10 K due to the presence of both insulating state in bulk and conductive state on the surface.

$$R + BCl_3 + H_2 \rightarrow RB_6\ (R = Nd, La_xPr_{1-x}) \quad (4)$$

In addition to the catalytic growth using metal particles (Au, Ni), there is also self-catalytic growth using rare-earth metals themselves as catalysts. In 2016, Han et al. reported the self-catalytic growth of NdB_6 and ternary $La_xPr_{1-x}B_6$ nanowires by an ordinary-pressure CVD method, as shown in Figure 2c,d [36,37]. Besides the NdB_6 nanowires, they also acquired NdB_6 nanoawls and nanotubes. The growth of ternary $La_xPr_{1-x}B_6$ nanowires reveals that this self-catalytic method is suitable for doping and preparation of RB_6 alloys.

2.2. HPSS Growth

Along with the CVD route, the solid-state method is also a route to prepare RB_6 crystals, including the high-pressure solid-state method [40–47], solution combustion method [48,49], and molten salt method [50,51]. However, because the diffusion rate of atoms in solid-state materials is extremely slow, it is difficult to obtain the nanowire morphology. At the same time, the low reactivity of solid source materials is also a problem restricting the development of 1D RB_6 nanomaterials. To solve such problems, from 2016, Zhao group utilized a rare-earth metal, self-catalytic, high-pressure solid-state method (HPSS) route to prepare various RB_6 nanowires, as shown in Figure 3a–f [52–57]. It is noteworthy that, until now, this is the only report on the synthesis of YbB_6 nanowires [56]. The general chemical reaction of the HPSS method is given below.

$$R + 6\ H_3BO_3 + 10\ Mg + I_2 \rightarrow RB_6 + 9\ MgO + MgI_2 + 9\ H_2O$$

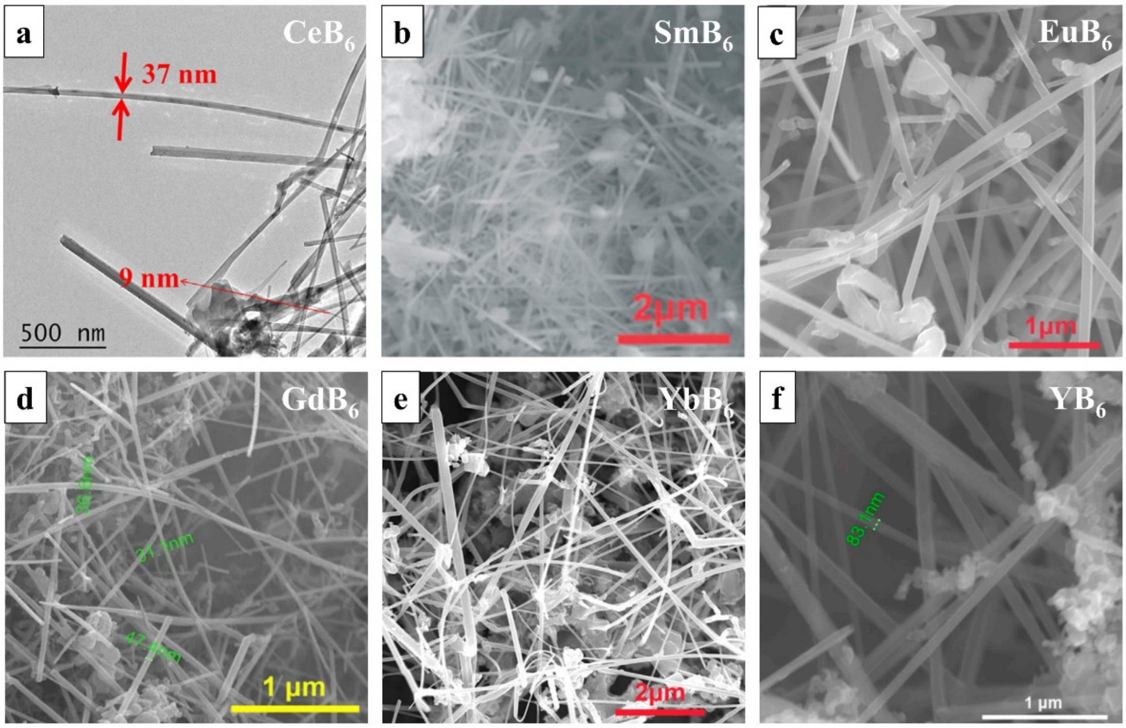

Figure 3. (**a**) TEM image of CeB_6 nanowires grown by HPSS method [52] (Copyright 2020, Elsevier Science B.V.). (**b**) SEM images of HPSS-grown SmB_6 nanowires [53] (Copyright 2016, The Royal Society of Chemistry). (**c**) EuB_6 nanowires [54] (Copyright 2021, Wiley-VCH GmbH). (**d**) GdB_6 nanowires [55] (Copyright 2017, Elsevier Science B.V.). (**e**) YbB_6 nanowires [56] (Copyright 2018, Elsevier Science B.V.). (**f**) YB_6 nanowires [57] (Copyright 2021, Elsevier Science B.V.).

In this equation, Mg is used for the reduction of H_3BO_3, and I_2 acts as the catalyst to boost the reaction of R and B atoms. From the literature, the Gibbs free energy (Δ_rG)

and heat function ($\Delta_r H$) of this equation are about -1900 kJ mol^{-1} and -2000 kJ mol^{-1}, respectively, demonstrating that the reaction is spontaneous and exothermic. Moreover, the high pressure in the autoclave is generated by iodine (higher than 45 atm), which is also a key to obtaining RB_6 nanowires. Due to high exothermic and high pressure, the trigger temperature of this HPSS method (200–260 °C) is generally much lower than that of the CVD method (950–1100 °C). From the ex situ time-dependent morphology study (5 min, 30 min, 360 min), we speculate that the growth of nanowires has three steps: (i) diffusion and reaction of R and B atoms; (ii) nucleation of RB_6 crystals; (iii) growth of RB_6 nanowires [53]. This HPSS route is a general method for the synthesis of rare-earth hexaborides, which we believe can be extended to the synthesis of other metal boride nanowires.

3. Properties and Applications of RB_6 Nanowires

3.1. Electronic Transportation

As an emerging topological insulator, many experiments and theoretical studies have been conducted on bulk SmB_6 single crystals [8]. From 2016, researchers began to investigate the novel electronic transport and magneto-transport properties of SmB_6 nanowires [37,38,53,58–62]. In 2017, Kong et al. reported the spin-polarized surface state transport of single SmB_6 nanowires (Figure 4a–c) [58]. Under 5 K, the resistance appears saturated and flat, indicating that the surface states control the transport behavior. The appearance of topological surface states is caused by the reversal of *d* and *f* electrons. The fitting of a temperature-dependent resistance curve reveals that SmB_6 nanowire has a bulk gap ~3.2 meV, which is opened by the hybridization of the 4*f* bands and 5*d* bands in SmB_6 nanowires. As shown in Figure 4c, the magnetoresistance (MR) of SmB_6 nanowires is negative and the MR shows no sign of saturation at high magnetic field up to 14 T. The negative MR indicates that this transport behavior is spin-dependent. Furthermore, the nonlocal tests reveal that the surface state transport of SmB_6 nanowires is spin-polarized. In another interesting work, Zhou et al. reported the positive planar Hall effect (PHE) of SmB_6 nanowires (Figure 4d–f) [59]. They found that as the temperature decreases, the amplitude increases sharply, but saturates at 5 K. This positive PHE is due to the surface states of SmB_6. In other studies, the researchers found the anomalous magnetoresistance and the hysteresis of magnetoresistance in SmB_6 nanowires [60–62].

In the RB_6 family, like SmB_6, YbB_6 is proposed to be a mixed-valent (Yb^{2+}/Yb^{3+}) topological insulator and demonstrates new quantum phenomena [63–65]. In 2018, Han et al. reported the semiconductor–insulator transition behavior in a YbB_6 nanowire (Figure 5) [55]. As shown in Figure 5b, as the temperature decreases from 300 to 2 K, the resistivity of the YbB_6 nanowire device undergoes a dramatic 49-fold increase ($\rho_{2\,K}/\rho_{300\,K} = 49$). They propose that the semiconductor–insulator transition is due to a small band gap opening at a low temperature induced by the slightly boron-rich or boron-deficient segments in YbB_6 nanowires. Furthermore, the magnetoresistance (MR) of the YbB_6 nanowire was tested with perpendicular magnetic field B = 0–7 T at various temperatures. As displayed in Figure 5c, the MR shows no sign of saturation at high magnetic field up to 14 T and has a linear dependence with B^2 at 2 K and 10 K, which follows Kohler's law. Because a semiconductor–insulator transition occurred at 2 K for YbB_6 nanowires, the hole-dominant transport is credible at 2 K and the transport at 10 K is electron-dominant.

Of all the metal borides, YB_6 bulk crystals have the second highest superconducting transition temperature of 7.2 K after MgB_2. More superconducting properties have been studied in bulk YB_6 single crystals, but the superconducting properties of YB_6 nanowires have not been reported. Recently, Wang et al. reported the synthesis of 1D YB_6 nanowires by a high-pressure solid-state method and studied their magnetic properties (Figure 6). The temperature-dependent magnetization under zero-field cooling and field cooling revealed that the YB_6 nanowires have a superconducting transition with T_c = 7.8 K. Meanwhile, they found that the YB_6 nanowires exhibited a peak effect in the superconducting state observed from the magnetic hysteresis loops obtained at 2 K and 10 K, indicating that YB_6 nanowires pertain to a type-II superconductor.

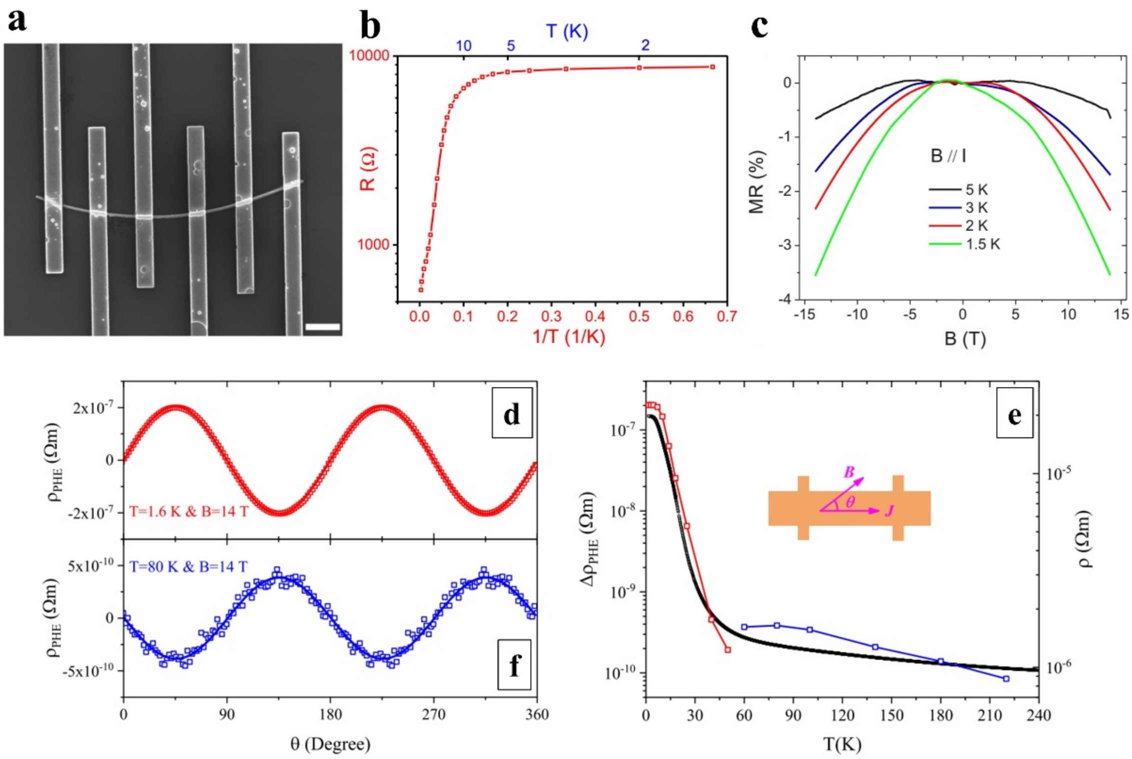

Figure 4. (**a**) SEM image of a SmB_6 nanowire device, the scalebar is 2 µm. (**b**) Temperature-dependent resistance of the SmB_6 nanowire. (**c**) Magnetoresistance curves under a parallel magnetic field at various temperatures [58]. Copyright 2017, American Physical Society. (**d**) Planar Hall resistivity with various angles at 1.6 K. (**e**) PHE amplitude and resistivity. Inset is the definition of tilting angle θ. (**f**) Planar Hall resistivity with various angles at 80 K [59]. Copyright 2019, American Physical Society.

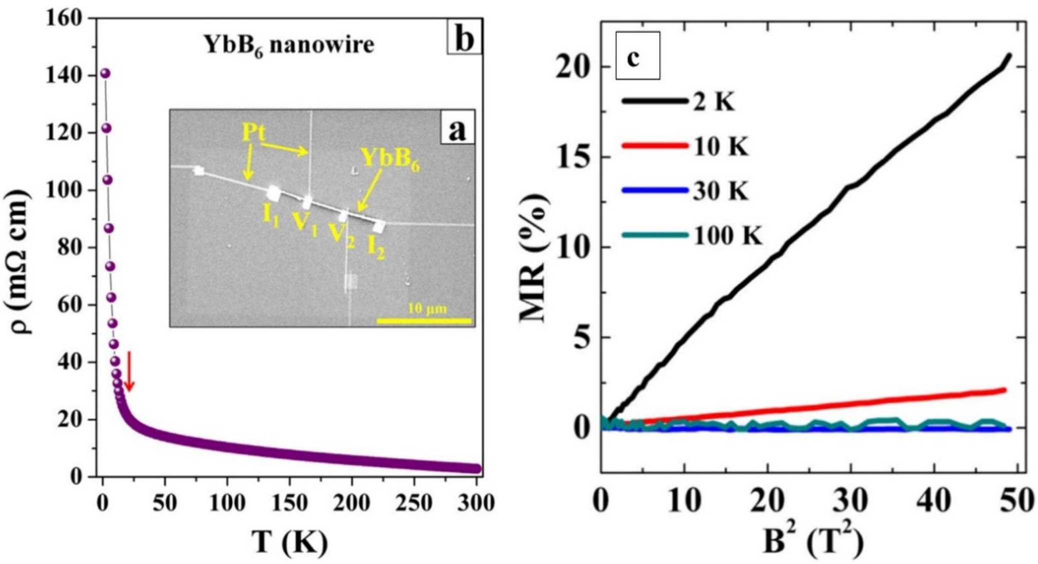

Figure 5. (**a**) SEM image of the YbB_6 nanowire device. (**b**) Resistivity as a function of temperature from 2 to 300 K. (**c**) Magnetoresistance (MR) as a function of B^2 at various temperatures [55]. Copyright 2018, Elsevier Science B.V.

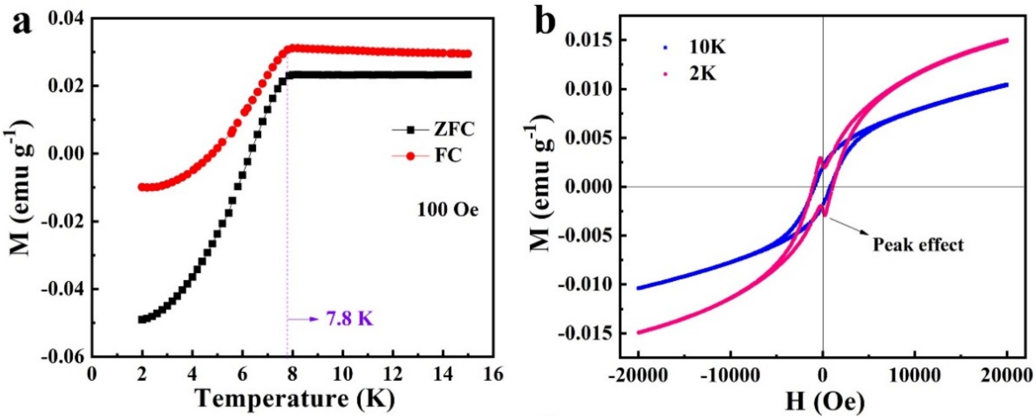

Figure 6. (**a**) The temperature-dependent magnetization under zero-field cooling and field cooling modes of superconducting YB_6 nanostructure. (**b**) The magnetic hysteresis loops obtained at 2 K and 10 K [57]. Copyright 2021, Elsevier Science B.V.

LaB_6 bulk single crystals have been applied in commercial scanning electron microscopy and transmission electron microscopy. For RB_6 nanowires, the most attractive application is also the field emitter of an electronic gun of an electron microscope (Figure 7) [66–68]. Published in Nature Nanotechnology, Zhang et al. reported the first application of a single LaB_6 nanowire to scanning electron microscopy, revealing excellent performance [66]. Their LaB_6 nanowire electron source shows low work function, is chemically inert, and has high monochromaticity. When assembled into a field-emission gun of SEM, it demonstrates ultra-low emission decay, and its current density gain is three orders of magnitude higher than traditional W tips. By this LaB_6 nanowire-based SEM, they obtained low-noise and high-resolution images, better than W-tip-based SEM. Recently, published in Nature Nanotechnology in 2021, Zhang et al. reported the installation of a single LaB_6 nanowire into an aberration-corrected transmission electron microscope [67]. The LaB_6 NW-based TEM achieved atomic resolution and probe-forming modes at 60 kV energy. Compared with the state-of-the-art W (310) electron source, the nanostructured electron source provides higher temporal coherence at a spatial frequency of 105 pm, showing a higher contrast transfer amplitude of 84% and a spectral energy resolution of 35%. The first demonstration of the LaB_6 nanowire electron source in SEM and TEM reveals that the RB_6 nanowires have notable application prospects and commercial value both in electron microscopy and other electron-emitting devices.

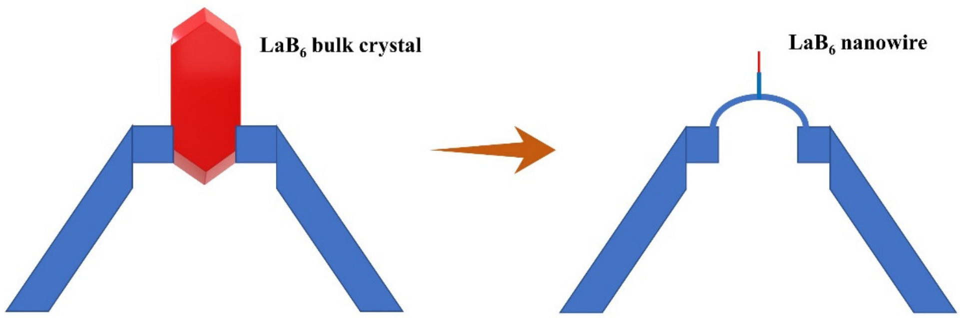

Figure 7. Illustrations of the LaB_6 bulk crystal and nanowire electron-emission sources in electron microscopy.

3.2. Optoelectronic Properties

Most of the RB_6 crystals are metals with zero band gap, and thus, they are not suitable for semiconductor devices, such as field effect transistors and photodetectors. However, as a topological Kondo insulator, SmB_6 shows a small gap (3 meV), evidenced by electrical transport measurements, and may have potential in fabricating devices. Recently, Zhou et al. [69] first reported the self-powered SmB_6 nanowire photodetectors with broadband wavelengths covering from 488 nm to 10.6 μm (Figure 8). They claimed that the photocurrent stemmed from the interface of SmB_6 nanowire and Au electrodes owing to the built-in potential, proved by the spatially resolved photocurrent mapping. The current on/off ratio, responsibility, and specific detectivity are 100, 1.99 mA/W, and 2.5×10^7 Jones, respectively. The demonstration of a SmB_6 nanowire photodetector reveals its application potential in mid-infrared photodetectors.

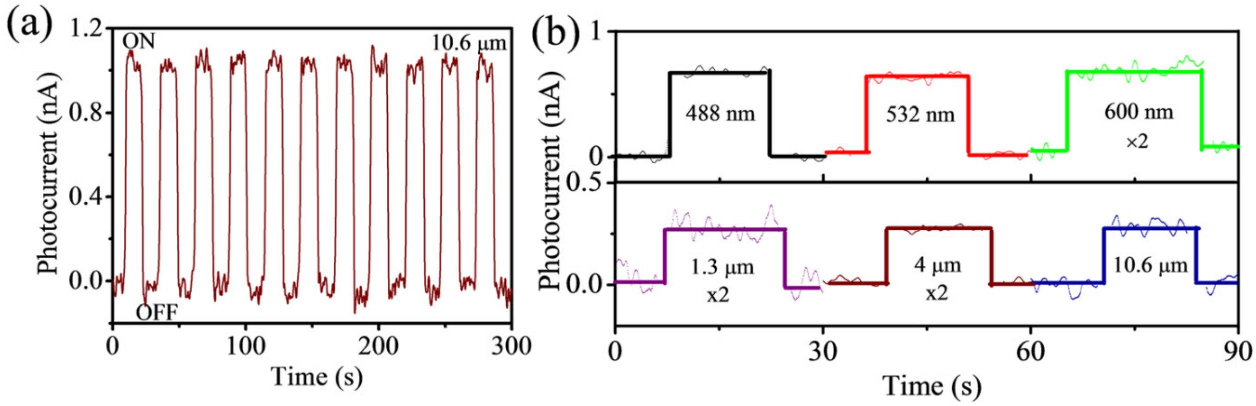

Figure 8. (**a**) Current–time measurement of SmB_6 nanowire photodetector under illuminating of 10.6 μm light source. (**b**) Current–time curves of SmB_6 nanowire photodetector under illuminating with different light wavelengths [69]. Copyright 2018, AIP Publishing.

3.3. Electrochemical Performances

RB_6 crystals show excellent metal-like conductivity (>10^3 S m^{-1}) and they are suitable for active electrochemical electrode materials for energy storage. Recently, Wang et al. [52] reported the application of CeB_6 nanowires as lithium-ion battery anode materials, and they obtained a capacity of ~225 mA h g^{-1} after 60 cycles (Figure 9a). The kinetic analysis shows that the Li^+ storage mechanism mainly comes from the surface capacitive behavior. Xue et al. [70] reported the LaB_6 nanowires on carbon fiber as electrode materials for supercapacitors (Figure 9b). The LaB_6 electrode materials showed a high areal capacitance of 17.34 mF cm^{-2} and revealed suitable cycling stability after 10,000 cycles. The successful application of RB_6 nanowires in batteries and capacitors demonstrates their potential in the field of electrochemical energy storage.

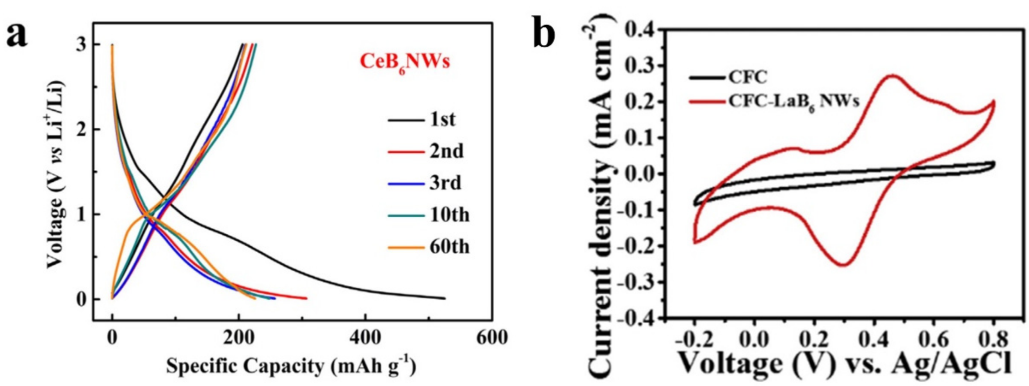

Figure 9. (**a**) The charge–discharge curves of CeB_6 nanowire electrodes for lithium-ion battery anodes [52]. (Copyright 2020, Elsevier Science B.V.) (**b**) CV curves of CFC and LaB_6-CFC electrode for supercapacitors [70]. (Copyright 2018, Elsevier Science B.V.)

4. Conclusions and Outlook

In conclusion, we review in this paper the recent developments in RB_6 nanowires in the past five years. Two main synthesis methods (CVD and HPSS) of RB_6 nanowires are outlined and compared. Moreover, their electronic transport, magnetic properties, and superconducting properties are summarized. Finally, the applications of RB_6 nanowires are revealed, including as field electron emitters, photodetectors, and in energy storage.

With the rise of two-dimensional (2D) materials, RB_6 nanowires should absorb some of the advantages of 2D material, such as atomically thin and large area lateral size. If RB_6 nanowires become thinner and wider, also called RB_6 nanobelts, they may reveal novel properties (Figure 10). In a recent study, Lee et al. reported the perfect Andreev reflection in a topological superconducting state based on SmB_6/YB_6 heterostructures [71]. We believe the heterostructures based on combinations of RB_6 nanowires or films may find new physical phenomena and represent future trends. In terms of the synthesis methods, CVD, solid-state, MBE, and PLD methods are all applicable, and only few improvements are needed. For instance, when using the CVD method to grow RB_6 nanobelts, mica substrates may be the best. Furthermore, adding some salts can improve the growth efficiency [72]. Meanwhile, 2D rare-earth materials have shown novel properties and applications, and thus, new discoveries and properties will also arise regarding the atomically thin 2D RB_6 nanobelts.

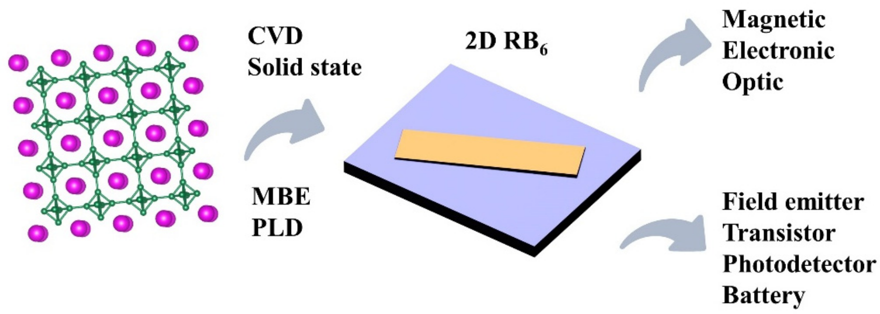

Figure 10. Outlook on the future growth, properties, and applications of RB_6 nanostructures.

Author Contributions: Writing—original draft preparation, Z.W., W.H.; writing—review and editing, Z.W., W.H.; supervision, W.H.; funding acquisition, W.H. All authors have read and agreed to the published version of the manuscript.

Funding: This research was funded by National Natural Science Foundation Committee of China (grant number 22105162).

Acknowledgments: The authors thank the grant from National Natural Science Foundation Committee of China (grant number 22105162).

Conflicts of Interest: The authors declare no conflict of interest.

References

1. Ji, X.H.; Zhang, Q.Y.; Xu, J.Q.; Zhao, Y.M. Rare-earth hexaborides nanostructures: Recent advances in materials, characterization and investigations of physical properties. *Prog. Solid State Chem.* **2011**, *39*, 51–69. [CrossRef]
2. Carenco, S.; Portehault, D.; Boissiere, C.; Mezailles, N.; Sanchez, C. Nanoscaled metal borides and phosphides: Recent developments and perspectives. *Chem. Rev.* **2013**, *113*, 7981–8065. [CrossRef] [PubMed]
3. Gan, H.; Zhang, T.; Guo, Z.; Lin, H.; Li, Z.; Chen, H.; Chen, J.; Liu, F. The growth methods and field emission studies of low-dimensional boron-based nanostructures. *Appl. Sci.* **2019**, *9*, 1019. [CrossRef]
4. Kunii, S.; Kasuya, T.; Kadowaki, K.; Date, M.; Woods, S.B. Electron tunneling into superconducting YB_6. *Solid State Commun.* **1984**, *52*, 659–661. [CrossRef]
5. Zhang, H.; Tang, J.; Zhang, Q.; Zhao, G.; Yang, G.; Zhang, J.; Zhou, O.; Qin, L.-C. Field emission of electrons from single LaB_6 nanowire. *Adv. Mater.* **2006**, *18*, 87–91. [CrossRef]
6. Jang, H.; Friemel, G.; Ollivier, J.; Dukhnenko, A.V.; Shitsevalova, N.Y.; Filipov, V.B.; Keimer, B.; Inosov, D.S. Intense low-energy ferromagnetic fluctuations in the antiferromagnetic heavy-fermion metal CeB_6. *Nat. Mater.* **2014**, *13*, 682–687. [CrossRef]
7. Pohlit, M.; Rößler, S.; Ohno, Y.; Ohno, H.; Von Molnár, S.; Fisk, Z.; Müller, J.; Wirth, S. Evidence for ferromagnetic clusters in the colossal-magnetoresistance material EuB_6. *Phys. Rev. Lett.* **2018**, *120*, 257201. [CrossRef] [PubMed]
8. Li, L.; Sun, K.; Kurdak, C.; Allen, J.W. Emergent mystery in the Kondo insulator samarium hexaboride. *Nat. Rev. Phys.* **2020**, *2*, 463–479. [CrossRef]
9. Zhang, H.; Zhang, Q.; Tang, J.; Qin, L.C. Single-crystalline LaB_6 nanowires. *J. Am. Chem. Soc.* **2005**, *127*, 2862–2863. [CrossRef]

10. Zhang, H.; Zhang, Q.; Tang, J.; Qin, L.C. Single-crystalline CeB_6 nanowires. *J. Am. Chem. Soc.* **2005**, *127*, 8002–8003. [CrossRef]
11. Zhang, H.; Zhang, Q.; Zhao, G.; Tang, J.; Zhou, O.; Qin, L.C. Single-crystalline GdB_6 nanowire field emitters. *J. Am. Chem. Soc.* **2005**, *127*, 13120–13121. [CrossRef]
12. Xu, J.; Zhao, Y.; Zou, C. Self-catalyst growth of LaB_6 nanowires and nanotubes. *Chem. Phys. Lett.* **2006**, *423*, 138–142. [CrossRef]
13. Zou, C.Y.; Zhao, Y.M.; Xu, J.Q. Synthesis of single-crystalline CeB_6 nanowires. *J. Cryst. Growth* **2006**, *291*, 112–116. [CrossRef]
14. Ding, Q.; Zhao, Y.; Xu, J.; Zou, C. Large-scale synthesis of neodymium hexaboride nanowires by self-catalyst. *Solid State Commun.* **2007**, *141*, 53–56. [CrossRef]
15. Xu, J.; Chen, X.; Zhao, Y.; Zou, C.; Ding, Q.; Jian, J. Self-catalyst growth of EuB_6 nanowires and nanotubes. *J. Cryst. Growth* **2007**, *303*, 466–471. [CrossRef]
16. Xu, J.Q.; Zhao, Y.M.; Shi, Z.D.; Zou, C.Y.; Ding, Q.W. Single-crystalline SmB_6 nanowires. *J. Cryst. Growth* **2008**, *310*, 3443–3447. [CrossRef]
17. Brewer, J.R.; Deo, N.; Wang, Y.M.; Cheung, C.L. Lanthanum hexaboride nanoobelisks. *Chem. Mater.* **2007**, *19*, 6379–6381. [CrossRef]
18. Wang, G.; Brewer, J.R.; Chan, J.Y.; Diercks, D.R.; Cheung, C.L. Morphological evolution of neodymium boride nanostructure growth by chemical vapor deposition. *J. Phys. Chem. C* **2009**, *113*, 10446–10451. [CrossRef]
19. Brewer, J.R.; Jacobberger, R.M.; Diercks, D.R.; Cheung, C.L. Rare earth hexaboride nanowires: General synthetic design and analysis using atom probe tomography. *Chem. Mater.* **2011**, *23*, 2606–2610. [CrossRef]
20. Chi, M.; Zhao, Y.; Fan, Q.; Han, W. The synthesis of PrB_6 nanowires and nanotubes by the self-catalyzed method. *Ceram. Int.* **2014**, *40*, 8921–8924. [CrossRef]
21. Zhang, H.; Tang, J.; Yuan, J.; Ma, J.; Shinya, N.; Nakajima, K.; Murakami, H.; Ohkubo, T.; Qin, L.-C. Nanostructured LaB_6 field emitter with lowest apical work function. *Nano Lett.* **2010**, *10*, 3539–3544. [CrossRef] [PubMed]
22. Xu, J.; Chen, X.; Zhao, Y.; Zou, C.; Ding, Q. Single-crystalline PrB_6 nanowires and their field-emission properties. *Nanotechnology* **2007**, *18*, 115621. [CrossRef]
23. Xu, J.Q.; Zhao, Y.M.; Zhang, Q.Y. Enhanced electron field emission from single-crystalline LaB_6 nanowires with ambient temperature. *J. Appl. Phys.* **2008**, *104*, 124306. [CrossRef]
24. Xu, J.Q.; Zhao, Y.M.; Ji, X.H.; Zhang, Q.; Lau, S.P. Growth of single-crystalline SmB_6 nanowires and their temperature-dependent electron field emission. *J. Phys. D Appl. Phys.* **2009**, *42*, 135403. [CrossRef]
25. Zhang, Q.Y.; Xu, J.Q.; Zhao, Y.M.; Ji, X.H.; Lau, S.P. Fabrication of large-scale single-crystalline PrB_6 nanorods and their temperature-dependent electron field emission. *Adv. Funct. Mater.* **2009**, *19*, 742–747. [CrossRef]
26. Xu, J.; Hou, G.; Li, H.; Zhai, T.; Dong, B.; Yan, H.; Wang, Y.; Yu, B.; Bando, Y.; Golberg, D. Fabrication of vertically aligned single-crystalline lanthanum hexaboride nanowire arrays and investigation of their field emission. *NPG Asia Mater.* **2013**, *5*, e53. [CrossRef]
27. Xu, J.; Hou, G.; Mori, T.; Li, H.; Wang, Y.; Chang, Y.; Luo, Y.; Yu, B.; Ma, Y.; Zhai, T. Excellent field-emission performances of neodymium hexaboride (NdB_6) nanoneedles with ultra-low work functions. *Adv. Funct. Mater.* **2013**, *23*, 5038–5048. [CrossRef]
28. Li, Q.; Zhang, H.; Chen, J.; Zhao, Y.; Han, W.; Fan, Q.; Liang, Z.; Liu, X.; Kuang, Q. Single-crystalline $La_xNd_{1-x}B_6$ nanowires: Synthesis, characterization and field emission performance. *J. Mater. Chem. C* **2015**, *3*, 7476–7482. [CrossRef]
29. Zhang, H.; Tang, J.; Zhang, L.; An, B.; Qin, L.C. Atomic force microscopy measurement of the Young's modulus and hardness of single LaB_6 nanowires. *Appl. Phys. Lett.* **2008**, *92*, 173121. [CrossRef]
30. Hossain, F.M.; Riley, D.P.; Murch, G.E. Ab initio calculations of the electronic structure and bonding characteristics of LaB6. *Phys. Rev. B* **2005**, *72*, 235101. [CrossRef]
31. Liu, H.; Zhang, X.; Ning, S.; Xiao, Y.; Zhang, J. The electronic structure and work functions of single crystal LaB_6 typical crystal surfaces. *Vacuum* **2017**, *143*, 245–250. [CrossRef]
32. Neupane, M.; Xu, S.Y.; Alidoust, N.; Bian, G.; Kim, D.J.; Liu, C.; Belopolski, I.; Chang, T.-R.; Jeng, H.-T.; Durakiewicz, T.; et al. Non-Kondo-like electronic structure in the correlated rare-earth hexaboride YbB6. *Phys. Rev. Lett.* **2015**, *114*, 016403. [CrossRef] [PubMed]
33. Dzero, M.; Xia, J.; Galitski, V.; Coleman, P. Topological kondo insulators. *Annu. Rev. Condens. Matter Phys.* **2016**, *7*, 249–280. [CrossRef]
34. Gan, H.B.; Peng, L.X.; Yang, X.; Tian, Y.; Xu, N.S.; Chen, J.; Liu, F.; Deng, S.Z. A moderate synthesis route of 5.6 mA-current LaB_6 nanowire film with recoverable emission performance towards cold cathode electron source applications. *RSC Adv.* **2017**, *7*, 24848–24855. [CrossRef]
35. Fu, C.; Xu, J.; Chang, Y.; Wang, Q.; Wang, Y.; Yu, B.; Guo, P.; Xu, J.; Sun, H.; Luo, Y.; et al. Flexible three-dimensional CeB_6 nanowire arrays and excellent field emission emitters. *J. Alloys Compd.* **2017**, *729*, 997–1003. [CrossRef]
36. Han, W.; Zhao, Y.; Fan, Q.; Li, Q. Preparation and growth mechanism of one-dimensional NdB_6 nanostructures: Nanobelts, nanoawls, and nanotubes. *RSC Adv.* **2016**, *6*, 41891–41896. [CrossRef]
37. Han, W.; Zhang, H.; Chen, J.; Zhao, Y.; Fan, Q.; Li, Q.; Liu, X.; Lin, X. Single-crystalline $La_xPr_{1-x}B_6$ nanoawls: Synthesis, characterization and growth mechanism. *Ceram. Int.* **2016**, *42*, 6236–6243. [CrossRef]
38. Gan, H.; Ye, B.; Zhang, T.; Xu, N.; He, H.; Deng, S.; Liu, F. A controllable solid-source CVD route to prepare topological Kondo insulator SmB_6 nanobelt and nanowire arrays with high activation energy. *Cryst. Growth Des.* **2019**, *19*, 845–853. [CrossRef]

39. Zhou, Y.; Peng, Y.H.; Yin, Y.L.; Zhou, W.C.; Zhou, F.; Liu, C.; Liu, G.T.; Sun, L.F.; Tang, D.S. Large-scale synthesis and electrical transport properties of single-crystalline SmB_6 nanowires. *J. Phys. D Appl. Phys.* **2016**, *49*, 265302. [CrossRef]
40. Selvan, R.K.; Genish, I.; Perelshtein, I.; Calderon Moreno, J.M.; Gedanken, A. Single step, low-temperature synthesis of submicron-sized rare earth hexaborides. *J. Phys. Chem. C* **2008**, *112*, 1795–1802. [CrossRef]
41. Zhang, M.; Yuan, L.; Wang, X.; Fan, H.; Wang, X.; Wu, X.; Wang, H.; Qian, Y. A low-temperature route for the synthesis of nanocrystalline LaB_6. *J. Solid State Chem.* **2008**, *181*, 294–297. [CrossRef]
42. Zhang, M.; Wang, X.; Zhang, X.; Wang, P.; Xiong, S.; Shi, L.; Qian, Y. Direct low-temperature synthesis of RB_6 (R = Ce, Pr, Nd) nanocubes and nanoparticles. *J. Solid State Chem.* **2009**, *182*, 3098–3104. [CrossRef]
43. Zhang, M.; Jia, Y.; Xu, G.; Wang, P.; Wang, X.; Xiong, S.; Wang, X.; Qian, Y. Mg-assisted autoclave synthesis of RB_6 (R = Sm, Eu, Gd, and Tb) submicron cubes and SmB_6 submicron rods. *Eur. J. Inorg. Chem.* **2010**, *8*, 1289–1294. [CrossRef]
44. Pol, V.G.; Pol, S.V.; Gedanken, A. Dry autoclaving for the nanofabrication of sulfides, selenides, borides, phosphides, nitrides, carbides, and oxides. *Adv. Mater.* **2011**, *23*, 1179–1190. [CrossRef]
45. Wang, L.; Xu, L.; Ju, Z.; Qian, Y. A versatile route for the convenient synthesis of rare-earth and alkaline-earth hexaborides at mild temperatures. *CrystEngComm* **2010**, *12*, 3923–3928. [CrossRef]
46. Chen, B.; Yang, L.; Heng, H.; Chen, J.; Zhang, L.; Xu, L.; Qian, Y.; Yang, J. Additive-assisted synthesis of boride, carbide, and nitride micro/nanocrystals. *J. Solid State Chem.* **2012**, *194*, 219–224. [CrossRef]
47. Zhou, L.; Yang, L.; Shao, L.; Chen, B.; Meng, F.; Qian, Y.; Xu, L. General fabrication of boride, carbide, and nitride nanocrystals via a metal-hydrolysis-assisted process. *Inorg. Chem.* **2017**, *56*, 2440–2447. [CrossRef] [PubMed]
48. Kanakala, R.; Rojas-George, G.; Graeve, O.A. Unique preparation of hexaboride nanocubes: A first example of boride formation by combustion synthesis. *J. Am. Ceram. Soc.* **2010**, *93*, 3136–3141. [CrossRef]
49. Kanakala, R.; Escudero, R.; Rojas-George, G.; Ramisetty, M.; Graeve, O.A. Mechanisms of combustion synthesis and magnetic response of high-surface-area hexaboride compounds. *ACS Appl. Mater. Inter.* **2011**, *3*, 1093–1100. [CrossRef]
50. Portehault, D.; Devi, S.; Beaunier, P.; Gervais, C.; Giordano, C.; Sanchez, C.; Antonietti, M. A general solution route toward metal boride nanocrystals. *Angew. Chem. Int. Ed.* **2011**, *50*, 3262–3265. [CrossRef]
51. Liu, X.; Gong, Y. Molten salt synthesis of samarium borides with controllable stoichiometry and morphology. *J. Alloys Compd.* **2021**, *867*, 159174. [CrossRef]
52. Wang, Z.; Han, W.; Kuang, Q.; Fan, Q.; Zhao, Y. Low-temperature synthesis of CeB_6 nanowires and nanoparticles as feasible lithium-ion anode materials. *Adv. Powder Tech.* **2020**, *31*, 595–603. [CrossRef]
53. Han, W.; Qiu, Y.; Zhao, Y.; Zhang, H.; Chen, J.; Sun, S.; Lan, L.; Fan, Q.; Li, Q. Low-temperature synthesis and electronic transport of topological insulator SmB_6 nanowires. *CrystEngComm* **2016**, *18*, 7934–7939. [CrossRef]
54. Wang, Z.; Han, W.; Fan, Q.; Zhao, Y. High-pressure growth and magnetic and electrical properties of EuB_6 nanowires. *Phys. Status Solidi (RRL) Rapid Res. Lett.* **2021**, *15*, 2100249. [CrossRef]
55. Han, W.; Wang, Z.; Li, Q.; Liu, H.; Fan, Q.; Dong, Y.; Kuang, Q.; Zhao, Y. Autoclave growth, magnetic, and optical properties of GdB_6 nanowires. *J. Solid State Chem.* **2017**, *256*, 53–59. [CrossRef]
56. Han, W.; Wang, Z.; Li, Q.; Lian, X.; Liu, X.; Fan, Q.; Zhao, Y. Semiconductor-insulator transition in a YbB_6 nanowire with boron vacancy. *J. Solid State Chem.* **2018**, *262*, 244–250. [CrossRef]
57. Wang, Z.; Han, W.; Zhang, J.; Fan, Q.H.; Zhao, Y.M. Superconducting YB_6 nanowires. *Ceram. Int.* **2021**, *47*, 23788–23793. [CrossRef]
58. Kong, L.J.; Zhou, Y.; Liu, S.; Lin, Z.; Zhang, L.; Lin, F.; Tang, D.S.; Wu, H.C.; Liu, J.F.; Lu, H.Z.; et al. Spin-polarized surface state transport in a topological Kondo insulator SmB_6 nanowire. *Phys. Rev. B* **2017**, *95*, 235410. [CrossRef]
59. Zhou, L.; Ye, B.C.; Gan, H.B.; Tang, J.Y.; Chen, P.B.; Du, Z.Z.; Tian, Y.; Deng, S.Z.; Guo, G.P.; Lu, H.Z.; et al. Surface-induced positive planar Hall effect in topological Kondo insulator SmB_6 microribbons. *Phys. Rev. B* **2019**, *99*, 155424. [CrossRef]
60. He, X.S.; Gan, H.B.; Du, Z.Z.; Ye, B.C.; Zhou, L.; Tian, Y.; Deng, S.Z.; Guo, G.P.; Lu, H.Z.; Liu, F.; et al. Magnetoresistance anomaly in topological Kondo insulator SmB_6 nanowires with strong surface magnetism. *Adv. Sci.* **2018**, *5*, 1700753. [CrossRef]
61. Kong, L.J.; Zhou, Y.; Song, H.D.; Yu, D.P.; Liao, Z.M. Magnetoresistance hysteresis in topological Kondo insulator SmB_6 nanowire. *Chin. Phys. B* **2019**, *28*, 107501. [CrossRef]
62. Gan, H.; Ye, B.; Zhou, L.; Zhang, T.; Tian, Y.; Deng, S.; He, H.; Liu, F. Controllable synthesis of Gd-doped SmB_6 nanobelt arrays for modulating their surface transport behaviors. *Mater. Today Nano* **2020**, *12*, 100097. [CrossRef]
63. Kang, C.J.; Denlinger, J.D.; Allen, J.W.; Min, C.H.; Reinert, F.; Kang, B.Y. Electronic structure of YbB_6: Is it a topological insulator or not? *Phys. Rev. Lett.* **2016**, *116*, 116401. [CrossRef] [PubMed]
64. Zhou, Y.; Kim, D.J.; Rosa, P.F.S.; Wu, Q.; Guo, J.; Zhang, S.; Wang, Z.; Kang, D.; Zhang, C.; Yi, W.; et al. Pressure-induced quantum phase transitions in a YbB_6 single crystal. *Phys. Rev. B* **2015**, *92*, 241118. [CrossRef]
65. Munarriz, J.; Robinson, P.J.; Alexandrova, A.N. Towards a single chemical model for understanding lanthanide hexaborides. *Angew. Chem.* **2020**, *132*, 22873–22878. [CrossRef]
66. Zhang, H.; Tang, J.; Yuan, J.S.; Yamauchi, Y.; Suzuki, T.T.; Shinya, N.; Nakajima, K.; Qin, L.C. An ultrabright and monochromatic electron point source made of a LaB_6 nanowire. *Nat. Nanotech.* **2016**, *11*, 273. [CrossRef]
67. Zhang, H.; Jimbo, Y.; Niwata, A.; Ikeda, A.; Yasuhara, A.; Ovidiu, C.; Kimoto, K.; Kasaya, T.; Miyazaki, H.T.; Tsujii, N.; et al. High-endurance micro-engineered LaB_6 nanowire electron source for high-resolution electron microscopy. *Nat. Nanotechnol.* **2021**, 1–6. [CrossRef]

68. Tang, S.; Tang, J.; Wu, Y.M.; Chen, Y.-H.; Uzuhashi, J.; Ohkubo, T.; Qin, L.-C. Stable field-emission from a CeB_6 nanoneedle point electron source. *Nanoscale* **2021**, *13*, 17156–17161. [CrossRef] [PubMed]
69. Zhou, Y.; Lai, J.W.; Kong, L.J.; Ma, J.C.; Lin, Z.L.; Lin, F.; Zhu, R.; Xu, J.; Huang, S.M.; Tang, D.S.; et al. Single crystalline SmB_6 nanowires for self-powered, broadband photodetectors covering mid-infrared. *Appl. Phys. Lett.* **2018**, *112*, 162106. [CrossRef]
70. Xue, Q.; Tian, Y.; Deng, S.Z.; Huang, Y.; Zhu, M.S.; Pei, Z.X.; Li, H.F.; Liu, F.; Zhi, C.Y. LaB_6 nanowires for supercapacitors. *Mater. Today Energy* **2018**, *10*, 28–33. [CrossRef]
71. Lee, S.; Stanev, V.; Zhang, X.; Stasak, D.; Flowers, J.; Higgins, J.S.; Dai, S.; Blum, T.; Pan, X.; Yakoveno, V.M.; et al. Perfect Andreev reflection due to the Klein paradox in a topological superconducting state. *Nature* **2019**, *570*, 344–348. [CrossRef] [PubMed]
72. Li, S. Salt-assisted chemical vapor deposition of two-dimensional transition metal dichalcogenides. *iScience* **2021**, *24*, 103229. [CrossRef] [PubMed]